# A 66 $\mu$W 86 ppm/°C Fully-Integrated 6 MHz Wienbridge Oscillator With a 172 dB Phase Noise FOM

Valentijn De Smedt, *Student Member, IEEE*, Pieter De Wit, *Student Member, IEEE*, Wim Vereecken, *Member, IEEE*, and Michiel S. J. Steyaert, *Fellow, IEEE*

*Abstract*—This paper presents the design of a new Wienbridge topology. Its phase noise performance, low temperature dependency and low power consumption make it suitable for use in wireless sensor nodes and time-based sensor readout circuitry. The noise as well as temperature behavior of the oscillator is explained using extensive calculations. Measurements on 7 samples of the same batch show a temperature stability of 86 ppm/°C and a measured spread of 0.9% at an oscillation frequency of 6 MHz. The circuit consumes 66 $\mu$W and is realized in a 65 nm technology measuring 150 $\mu$m by 200 $\mu$m. The measured phase noise figure of merit is 172 dB at a frequency offset of 100 kHz.

*Index Terms*—Harmonic oscillator, oscillator noise, oscillator topology, RF, ultra-low-power, Wienbridge.

### LIST OF SYMBOLS

| | |
|---|---|
| $T(s)$ | Loop-gain of a feedback system. |
| $H(s)$ | Transfer function of a resonant network. |
| $G(s)$ | Forward amplifier gain. |
| $Q$ | Quality factor of a resonator/system. |
| $Q_G$ | Generalized Q-factor of a system. |
| $R$ | Resistor in the feedback network. |
| $C$ | Capacitor in the feedback network. |
| $r_o$ | Output resistance of the amplifier. |
| $R_{\text{tot}}$ | Output resistance of the amplifier with feedback network ($= R//r_o$). |
| $R_{\text{deg}}$ | Source degeneration resistance. |
| $g_m$ | Transconductance of a transistor. |
| $g_{m,\text{deg}}$ | Transconductance of a source-degenerated transistor. |
| $V(t)$ | Complex representation of a voltage oscillation. |
| $v(t)$ | Real representation of a voltage oscillation. |

## I. INTRODUCTION

INTEGRATION of complete systems on a single chip is one of the most important evolutions in modern micro-electronics. Fully integrated systems-on-chip, including both analog and digital circuits, are necessary to obtain high performance, power-efficient and low cost systems. On wireless nodes for instance, where PLL- or time-based sensors [1], RF-transmitters and low-power digital are embedded on a single chip [2], all the off-chip components such as an external crystal need to be eliminated. Regarding these issues, the need for temperature stable, accurate, fully integrated, low-power clock references arises. In applications with down mixing, the phase noise and amplitude stability of the oscillator also become important specifications [3], [4].

In deep-submicron processes, the spread on active components due to mismatch, temperature and other external parameters is very large and difficult to control. Passive devices on the other hand, are much more predictable and controllable, providing a better starting point for this kind of oscillator. The design methodology used in this paper is based on the principles that the frequency should only be determined by passive components (R, C, L) and that the influence of active components on the oscillation frequency should be minimized.

As will be pointed out in Section II-A, oscillators can be based on different passive components. Although some accurate relaxation oscillators are reported [5] and [6], their waveform is not suitable for down mixing purposes. In a mixed signal environment however, a harmonic oscillator can provide a digital clock as well as an analog, harmonic waveform. Since a low-power, low-frequency time reference is needed in e.g. a wireless sensor network [7] and [8], RC-based oscillators are preferred rather than the LC-based topologies. A solution for this kind of application can be found using a well-known harmonic oscillator structure: the Wienbridge oscillator [9]–[11]. The use of an improved topology makes it possible to realize a low phase-noise and temperature insensitive Wienbridge oscillator. In this new topology, the oscillator properties only depend on the passive (RC) feedback network.

Section II of this paper describes the general conditions for oscillation. The Q-factor and generalized Q-factor are defined and used to derive the frequency versus amplitude behavior of the oscillator. Section III handles the problem with the common Wienbridge topology in nanometer CMOS. Section IV discusses the alternative Wienbridge oscillator topology. The amplitude regulator incorporated in the oscillator is investigated in Section V. In Section VI the noise sources in the oscillator network are described. Simulation and measurement results are presented and compared in Section VII. Finally, some conclusions are drawn in Section VIII.

## II. CONDITIONS FOR OSCILLATION

In this section, some basic principles for oscillation will be reviewed, providing insight in the oscillation behavior. These insights will be indispensable to make the right design decisions in order to obtain a frequency-stable oscillator.

### A. General Considerations

To obtain a time reference, one or more energy tanks are required. An energy reservoir is able to exchange energy with another component which may be either another energy reservoir or a resistive element, e.g. a resistor. In case two different energy reservoirs are used there will be an energy conversion during the energy exchange. This conversion will happen with a certain time constant depending on the properties of the two energy reservoirs. An example of this is the LC-oscillator, in which energy is exchanged between the magnetic field of an inductor and the electric field of a capacitor. In the other case, the use of an energy reservoir and a resistor will also provide a time constant. Examples are a capacitor or inductor and a resistor. Note that this resistor may as well be implemented with a current source and a reference voltage. Most relaxation oscillators are based on this working principle. The energy exchange between two energy reservoirs from the same type without the use of any other regulating element happens, theoretically, in an infinitely short time period. In this case it is not possible to derive a time constant or oscillator.

In literature a distinction is made between harmonic oscillators and relaxation oscillators. Although the previous discussion is valid for both cases, there is a difference in the way the energy reservoirs are used. In the relaxation oscillator only one energy reservoir is needed in combination with a resistive element and a nonlinear component (e.g. a transistor). A typical property of a relaxation oscillator is the current through or voltage over the energy reservoirs which is switched at certain reference levels. In this way discontinuous waveforms or waveforms with a discontinuous first derivative can be generated. In the case of harmonic oscillators two or more energy reservoirs are required. The energy reservoirs can either be of a different type or of the same type, if combined with a resistive element. Important to note is that these kinds of oscillators can be built by using only linear components and hence are only producing sine waves.

Note that these considerations and conditions for oscillation are valid for electrical oscillators as well as for mechanical and even for optical oscillators. Every time constant in nature can be reduced to one of the possibilities described above. The Wienbridge oscillator is a harmonic oscillator with two resistors and two capacitors.

### B. The Barkhausen Criterion

An oscillator may be described as a feedback system. As a condition to sustain oscillation, positive feedback is needed at a certain frequency, the oscillation frequency. The Barkhausen criterion states that for stable oscillation (i.e. oscillation with a constant amplitude), the loop-gain $T(s)$ of the system has to be equal to 1 and the phase shift has to be an integer multiple of $2\pi$ ($z \in \mathbb{Z}$):

$$\begin{cases} |T(s)| = 1 \\ \angle T(s) = z \cdot 2 \cdot \pi \end{cases} \tag{1}$$

Because of the nonlinear behavior of relaxation oscillators, they cannot be described using transfer functions. As such it is not possible to use the Barkhausen criterion to determine the oscillation frequency. However, in the case of harmonic oscillators, which can be described as linear systems, at least in their start up operating point, the Barkhausen criterion is a necessary condition for oscillation.

### C. The Q-Factor

The Q-factor or Quality factor of an oscillator is a dimensionless parameter comparing the rate of energy dissipation of a system to its oscillation frequency. For physical systems the Q-factor is generally defined as

$$Q = \omega \cdot \frac{E_{\text{stored}}}{P_{\text{loss}}} \tag{2}$$

$$= 2 \cdot \pi \cdot \frac{E_{\text{stored}}}{E_{\text{Dissipated-per-Cycle}}}. \tag{3}$$

One can prove (see Section II-D) that for a critically damped system the Q-factor equals 1/2. Resonators with a larger Q-factor are underdamped and show an oscillation with decreasing amplitude while returning to their equilibrium situation. Overdamped systems ($Q < 1/2$) do not oscillate on their own.

The definition can be used to calculate the Q-factor of different types of oscillators. In some cases however, it is nontrivial to calculate the stored energy or energy dissipation because of a combination of energy tanks which are charged at different moments in the oscillation cycle. In [12] two alternative methods are described to calculate the Q-factor of a resonator. The Q-factor can be calculated as function of the $-3$ dB width of the peak in the transfer function ($\Delta\omega$) and as a function of the steepness of the transfer function phase ($d\angle H(j\omega)/d\omega$) where it crosses $0^\circ$.

A final way to determine the Q-factor of a resonator is based on the resonator's transfer function. In general the transfer function of a second order harmonic resonator may be written as follows:

$$H(s) = \frac{K \cdot \omega_n \cdot s}{s^2 + \frac{\omega_n}{Q} \cdot s + \omega_n^2} \tag{4}$$

where $\omega_n$ is the resonant frequency of the resonator and K is a non-imaginary constant. In this way the Q-factor can be easily extracted. Note that high-Q resonators ($Q > 1/2$) can, due to their pairs of complex conjugated poles, always unambiguously be written as a product of second order systems. In low-Q systems one can calculate a Q-factor for each pair of poles. The noise and stability behavior is determined by the Q-factor of all

pairs of poles and the poles and zeros around the resulting oscillation frequency. However, in systems with more then 2 frequency determining poles or zeros it is more likely to use one of the other methods to calculate the resulting Q-factor.

### D. Frequency Versus Amplitude Stability

The Barkhausen criterion is fulfilled for a system when the transfer function $H(s)$ of the resonant network times the (complex) forward amplifier gain $G(s)$ equals 1 (Fig. 1).

$$\frac{K \cdot \omega_n \cdot s}{s^2 + \frac{\omega_n}{Q} \cdot s + \omega_n^2} \cdot G(s) = 1 \qquad (5)$$

This expression is the Laplace transform of the differential equation of a generic oscillator in time domain.

$$\omega_n^2 \cdot v(t) + \omega_n \cdot \left(\frac{1}{Q} - K \cdot G\right)\frac{dv(t)}{dt} + \frac{d^2v(t)}{dt^2} = 0 \qquad (6)$$

Note that the amplifier's transfer function $G(s)$ can be approximated by $G$ as long as the phase shift of the amplifier is negligible at the oscillation frequency, i.e. the amplifier or active components have no influence on the oscillator behavior. The solution to this differential equation can be simplified by defining the generalized Q-factor as

$$Q_G \triangleq \left(\frac{1}{Q} - K \cdot G\right)^{-1} \qquad (7)$$

When the feedback gain $G$ is zero, the generalized Q-factor is equal to the Q-factor of the passive resonator. After substitution of $Q_G$ in (6), the general solution of the differential equation becomes:

$$V(t) = A \cdot exp\left(\frac{-\omega_n \cdot t}{2Q_G}\right) \cdot exp\left(\frac{\sqrt{1 - 4Q_G^2}}{2Q_G} \cdot \omega_n \cdot t\right)$$
$$+ B \cdot exp\left(\frac{-\omega_n \cdot t}{2Q_G}\right) \cdot exp\left(-\frac{\sqrt{1 - 4Q_G^2}}{2Q_G} \cdot \omega_n \cdot t\right) \qquad (8)$$

where A and B are coefficients depending on the boundary conditions of the differential equation. Depending on the value of $Q_G$, a different behavior is observed. If $0 < Q_G < 1/2$, the solution is the sum of two real exponential functions. The system is overdamped and will not oscillate while returning exponentially to its equilibrium. When $Q_G = 1/2$, the system is critically damped. Under the same starting conditions, the critically damped system always returns faster to its equilibrium than the overdamped system. An oscillation is observed when

$$|Q_G| > \frac{1}{2}. \qquad (9)$$

In this case the solution contains a time varying complex exponential function, which means the system is oscillating over time. The real part of the generic solution can then be written as

$$v(t) = A' \cdot exp\left(\frac{-\omega_n \cdot t}{2Q_G}\right) \cdot sin\left(\frac{\sqrt{4Q_G^2 - 1}}{2Q_G} \cdot \omega_n \cdot t\right)$$
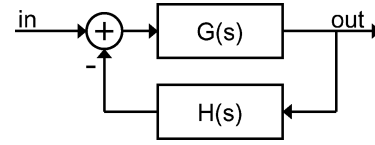


Fig. 1.   Overview of a general feedback system showing the amplifier and feedback network.

$$+ B' \cdot exp\left(\frac{-\omega_n \cdot t}{2Q_G}\right) \cdot cos\left(\frac{\sqrt{4Q_G^2 - 1}}{2Q_G} \cdot \omega_n \cdot t\right) \qquad (10)$$

where $A'$ and $B'$ are coefficients depending on the boundary conditions of the differential equation. A stable oscillation is observed, i.e. The Barkhausen criterion is fulfilled, when $s = j\omega_n$ (5) or $Q_G = \infty$. In the time domain (8) this corresponds to an oscillation at frequency $2\pi\omega_n$ with a constant amplitude $\sqrt{A'^2 + B'^2}$. When $G > 1/KQ$, the Barkhausen criterion is no longer fulfilled and $Q_G < 0$. In the Laplace domain this can be represented by (5) where the right hand side is changed to a number larger than one. The amplitude of the oscillation will increase. When the gain $G$ is high enough ($-1/2 < Q_G < 0$), the solution (8) becomes an increasing exponential function. In this case there is no oscillation and the output voltage approaches infinity. For oscillators with decreasing amplitude, $1/2 < Q_G < \infty$. This case can be represented by (5) where the right hand side is changed to a number lower than one.

An important conclusion from (10) is that in both cases, increasing and decreasing amplitude, the oscillation frequency is lower than in the case of a constant amplitude. This stresses the great importance of a stable amplitude regulation.

## III. THE WIENBRIDGE OSCILLATOR

### A. Ideal Wienbridge Oscillator

The Wienbridge oscillator is a harmonic oscillator consisting of 2 building blocks: an amplifier and a passive RC-feedback network (Fig. 2). The transfer function of the feedback network can be written as

$$H(s = j \cdot \omega) = \frac{s \cdot R \cdot C}{1 + 3 \cdot s \cdot R \cdot C + s^2 \cdot R^2 \cdot C^2}. \qquad (11)$$

The magnitude and phase behavior are displayed in Figs. 3 and 4. The Barkhausen criterion is fulfilled when an amplifier with a gain of 3 and zero phase shift is used. This results in the following oscillation frequency:

$$f = \frac{1}{2 \cdot \pi \cdot R \cdot C} \qquad (12)$$

in which $R$ and $C$ are the values of the resistors and capacitors in the feedback network. In the basic implementation (Fig. 2) the amplifier consists of an opamp and two feedback resistors to adjust the gain to 3. The Q-factor of this harmonic oscillator is easily extracted from (11):
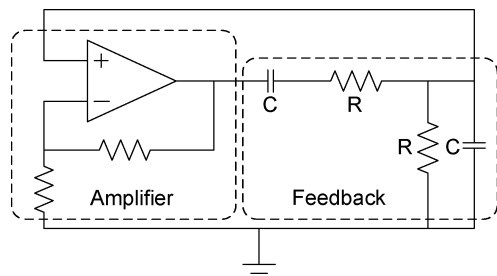
$$Q = 1/3 \qquad (13)$$

Fig. 2. Conventional Wienbridge topology using a passive feedback network and an opamp. Due to the feedback resistors, the amplifier has a gain of 3.
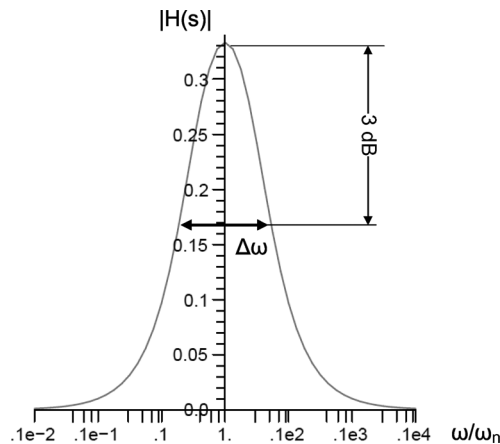


Fig. 3. Magnitude of the transfer function of the Wienbridge oscillator. The elements for the first definition of the Q-factor are indicated on the figure.
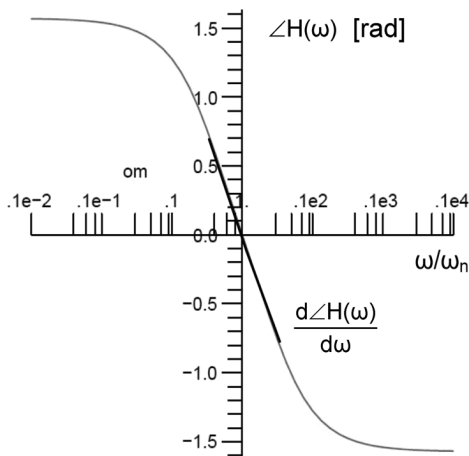


Fig. 4. Phase of the transfer function of the Wienbridge oscillator. The slope of the transfer function is indicated on the figure.

Note that the other two methods proposed in Section II-C result in the same Q-factor.

### B. Frequency Determining Factors

It is clear that in this ideal implementation, the oscillation frequency is only dependent on the passive RC network, as proposed in our design methodology (Section I). If a temperature independent oscillation is required, this network should consist of temperature stable passive elements. In the technology

used, N- and P-poly resistors and MIM-capacitors are available. The temperature dependency of the capacitors is considered negligible. Since the N- and P-poly resistors have a positive and a negative first-order temperature dependency respectively, a combined resistor with the remaining second-order temperature dependence is obtained. The ratio of the ideal N- to P-poly resistance was simulated to be approximately 2/3. The resulting temperature coefficient (36 ppm/°C) allows its use in a temperature stable oscillator topology.

For the resistors, [13] and [14] report a relative resistor mismatch ($3\sigma$) lower than 1% for resistor values higher than 20 k$\Omega$ and a width of 500 nm. The matching of the MIM-Capacitors is, due to their large dimensions (19.75 $\mu$m $\times$ 21 $\mu$m for the frequency determining capacitor C), expected to be 0.05% in a 130 nm technology [15]. Matching performance usually becomes better towards deep submicron, but for the worst case the above numbers are used (since process variation of the used technology was not available during the design). The expected mismatch in oscillation frequency (12) resulting from these figures within one wafer is about 1.1%. In order to have a high absolute accuracy over different runs, the absolute accuracy of the passives has to be guaranteed. Although the measurements in Section VII show some results close to the simulated values, the expected wafer-to-wafer frequency mismatch is 10 to 15 times higher [14]. For each wafer some trimming could possibly be required.

The use of a N- and P-poly combination to obtain a temperature independent resistance is based on their respective temperature coefficients. However, the temperature variation of both N- and P-poly resistors is only 2% over a temperature span of 140°C. In case of a 10% resistor mismatch, this results in a temperature dependency of only 0.2%, which corresponds to an extra 14 ppm/°C. As will be shown in Section VII this is only one third of the deviation caused by the amplitude regulator.

### C. Implementation Non-Idealities

Using an non-ideal opamp introduces the finite output impedance and phase shift to the transfer function. The output impedance becomes part of the feedback circuit, thereby becoming a determining parameter for the oscillation frequency. Since the output resistance of the transistors changes considerably with temperature and the pole frequencies in the amplifier (controlling the phase shift of the amplifier) are also very temperature dependent, this poses a serious problem for temperature-stable oscillation: the opamp becomes the critical part of the oscillator circuit. A temperature stable oscillator using the conventional Wienbridge topology implies the use of a very high performance opamp or alternative opamp configurations [11]. This, in turn, severely limits the low-power operating capabilities of such a circuit.

The impact of process variability makes matters even worse. The gain, output impedance and phase shift will have wide distributions, which has a large impact on the absolute accuracy of the oscillation frequency.

To avoid this trade-off between power consumption, temperature stability and absolute accuracy, a new topology has been developed.
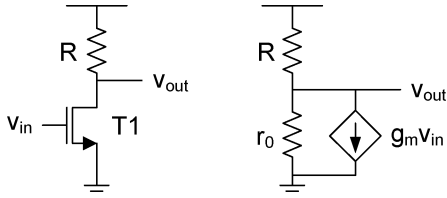
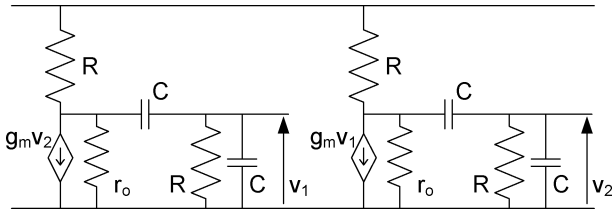Fig. 5. Schematic and small-signal model of a common source amplifier with drain resistor.



Fig. 6. Improved Wienbridge oscillator topology.



Fig. 7. Completed amplifier used in the Wienbridge oscillator.

## IV. IMPROVED WIENBRIDGE TOPOLOGY

### A. Basic Structure

As explained in the previous section, the amplifier is the critical component in the Wienbridge oscillator. The requirements can be summarized as follows: (1) a constant output impedance, (2) no phase shift at $f = f_{osc}$ and (3) a non-inverting voltage gain of 3. It is clear that these conditions have to be preserved under changing temperatures and process variability.

The amplifier needed can be easily realized using a simple common source transistor $T_1$ with drain resistor, as shown in Fig. 5. The drain resistor $R$ becomes, together with the output resistance of the transistor $r_o$ part of the feedback network. Since the total output resistance $R_{tot} = R//r_o$ determines the oscillation frequency and $r_o$ strongly varies with temperature, $R_{tot}$ should only be determined by the temperature stable resistor $R$. This is achieved by maximizing the output resistance of the amplifier $r_o$ by adding two cascode transistors. In this way the total, equivalent resistance $R_{tot}$ is almost independent of $r_o$, the output resistance of the transistor-branch.

The phase shift of the amplifier should be minimized at the oscillation frequency and is determined by the pole-frequencies of the amplifier. Since poles exist at the sources of the cascode transistors, their sizes should be limited ($W/L = 3 \times 0.475 \ \mu m/0.565 \ \mu m$).

A solution to the inverting behavior of the amplifier can be found in cascading two (inverting) amplifiers with feedback network, as shown in Fig. 6. The result is a loop of two Wienbridge oscillators. A differential signal will be found between the output nodes of the two amplifiers.

### B. Stability of the Voltage Gain: Source Degeneration

In a Wienbridge oscillator, a voltage gain of 3 is required. The voltage gain of the common source amplifier can be described as

$$A = g_m \cdot (R//r_o) \qquad (14)$$
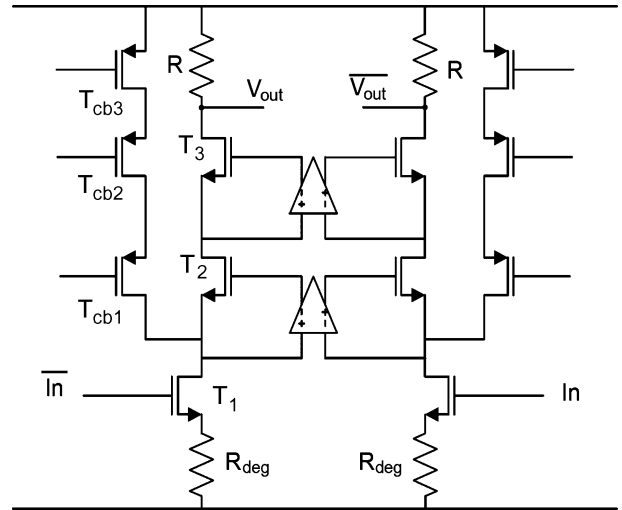
in which $g_m$ is the transconductance of the transistor.

As stated before, the output resistance of the transistor branch $r_o$ is maximized, resulting in an amplifier output resistance, determined by resistor $R$, which is strongly temperature independent. In contrast, the transconductance of the transistor $g_m$ varies as much as 35% over a temperature range of $-40$ to $100°C$, resulting in a large fluctuation of the gain.

In order to stabilize this gain, source degeneration is used. Using this technique, the transconductance of the amplifier becomes

$$g_{m,deg} = \frac{g_m}{1 + g_m \cdot R_{deg}} \approx \frac{1}{R_{deg}} \qquad (15)$$

which is largely determined by the source resistor $R_{deg} = 11.94 \ k\Omega$, a very temperature independent component (Fig. 7). This source degeneration also results in an increase of output resistance by a factor $(1 + g_m \cdot R_{deg})$, which is favorable. Apparently there is a trade-off between the magnitude and the temperature stability of the transconductance. In order to have a stable oscillation, a gain of 3 should be preserved. As the transconductance of a transistor can be written as

$$g_m = \frac{2 \cdot I_{ds}}{V_{gs} - V_{th}} \qquad (16)$$

an increased current through the common source transistor is needed to enhance $g_m$ and $g_{m,deg}$. Since, given a certain DC-biasing, the output resistance will drop inversely proportional to the transistor current, the amplifier gain (equal to $g_{m,deg} \times R$) is not affected by the increased biasing current.

### C. Increase of the Gain: Current Bleeding

A solution to the previous problem is found in the current bleeding technique. Using this technique, extra current can be delivered to the common source transistor (increased $g_m$), without increasing the current through the cascodes (output resistance preserved) and output resistor R. To minimize the impedance reduction at the current bleeding node, two cascode transistors $T_{cb,1}, T_{cb,2}$ are added to the inserted current sources $T_{cb,3}$ (see Fig. 7). The resulting amplifier has a temperature-stable voltage gain of 3. Due to the high output impedance
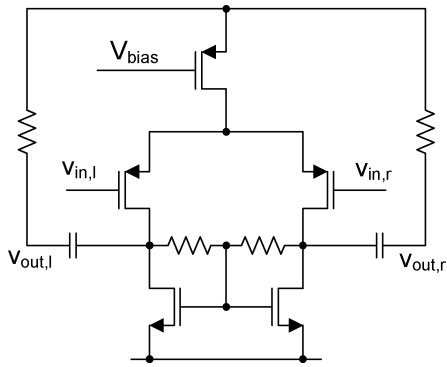
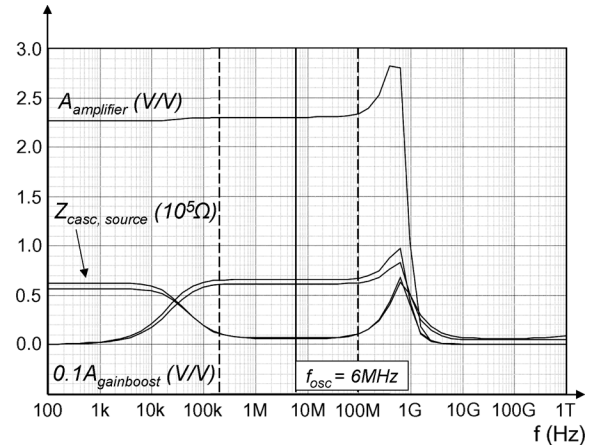Fig. 8. Gainboosting amplifier for the lower cascode transistors.



Fig. 9. A Bode plot showing the gain of the gainboosting amplifiers and the complete amplifier. The source impedance of the cascode transistors is also shown. The dashed lines indicate the active region of the gain boosters.

of the transistor branch (the transconductance amplifier), the output impedance of the amplifier is equal to $R$.

### D. Controlling the Output Resistance: Gain Boosting

To increase the output resistance of the transconductance amplifier even more, gain boosting has been applied to both cascode transistors. This results in an additional increase of the output resistance with a factor which is approximately equal to A, being the voltage gain of the gain-boosting amplifier. Gain boosting also has a positive effect on the phase shift of the amplifier: since the impedance at the source of the gain-boosted cascode transistor is reduced, its pole will shift towards a higher frequency, which will reduce the phase shift of the amplifier at the oscillation frequency significantly.

For reasons of compatibility with the differential architecture of the oscillator, the gain-boosting amplifiers have been implemented as fully differential amplifiers. The gain-boosting amplifier used on the lower cascode is shown in Fig. 8. The input $(v_{in,l}, v_{in,r})$ and output $(v_{out,l}, v_{out,r})$ terminals are respectively connected to the sources and gates of the cascode transistors, as shown in Fig. 7 showing the complete amplifier. The gain-boosting amplifier used on the upper cascode is similar, but uses a NMOS-differential pair. Due to the limited supply voltage in 65 nm, capacitive coupling between the output of the gain-boosting amplifiers and the gate terminals of the cascode transistors is used.

The resulting amplifier is shown in Fig. 7. It has a phase shift $< 0.4°$ until a frequency of 24 MHz and $< 2.1°$ at 48 MHz, resulting in a negligible phase shift at the oscillation frequency of 6 MHz. Note that even in a 48 MHz oscillator, the amplifier should hardly have an influence on the oscillation frequency.

The Bode plot, in Fig. 9, shows that the active frequency span of the gainboosting amplifiers $(A_{\text{gainboost}})$ ranges from 200 kHz to 100 MHz (dashed lines). In addition, the reduction of the source impedance of the cascode transistors $(Z_{\text{source,casc}})$ near the oscillation frequency is also shown on the graph. Finally, the overall gain of the amplifier $(A_{\text{amplifier}})$ is visualized.

Under all circumstances the simulated ratio between the transistor branch output resistance and the output resistor value R is higher than 1000.

### E. Guaranteeing the Absolute Accuracy

A lot of design decisions have been made to reduce the influence of the transistor branch on the oscillation frequency. This

also has serious advantages concerning the absolute accuracy of the oscillation frequency. Since this frequency is purely dependent on the passive components of the feedback network, the accuracy of $f_{osc}$ will depend on the spread on the value of these components. In a CMOS technology, the spread of passive components is due to their bigger size typically significantly smaller compared to active components [16]. Furthermore, as stated before, the temperature dependency of these components can be reduced significantly compared to that of the active components.

### V. THE AMPLITUDE REGULATOR

### A. Purpose and Stability Problem

To make sure the output impedance of the transistor branch remains high, the transistors have to operate in the saturation region. This means that the output amplitude has to be limited prior to the deformation of the output signal. This is only possible with a non-linear circuit which influences the gain of the Wienbridge amplifier. Typically an amplitude regulation circuit consists of three parts: 1) measurement of the amplitude by peak detection, 2) integration of the peak signal on a capacitor, and 3) feedback to the gain of the amplifier. As described in [17] one of the main problems of amplitude regulation with peak detection is its instability. A first pole in the feedback network can be found in the integrator. The second pole appears due to the delay between the gain adaptation and the amplitude change. This is, in a harmonic oscillator, a consequence of the finite Q-factor of the resonator [18]. As proved in Section II-D an instability in the amplitude regulation will cause a time varying shift on the oscillators frequency. Certainly in applications where a high frequency accuracy is required or where down mixing is used this is not acceptable for obvious reasons.

### B. Proposed Solution and Implementation

One solution to cope with this instability problem is providing a shortcut around the second pole for high amplitudes. If the peak detection circuit immediately influences the oscillation amplitude, this shortcut is realized. In the realized amplitude regulator, the signal peaks are compared to a reference voltage $V_{ref}$ which is generated using a replica of the amplifier
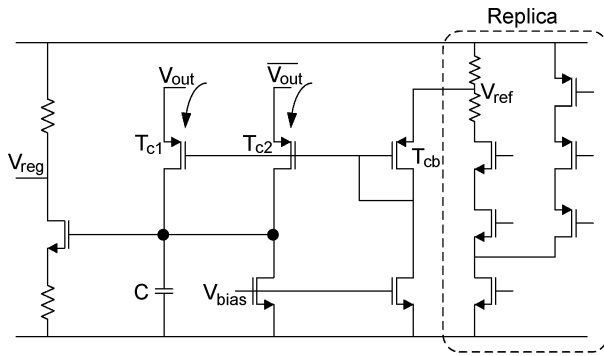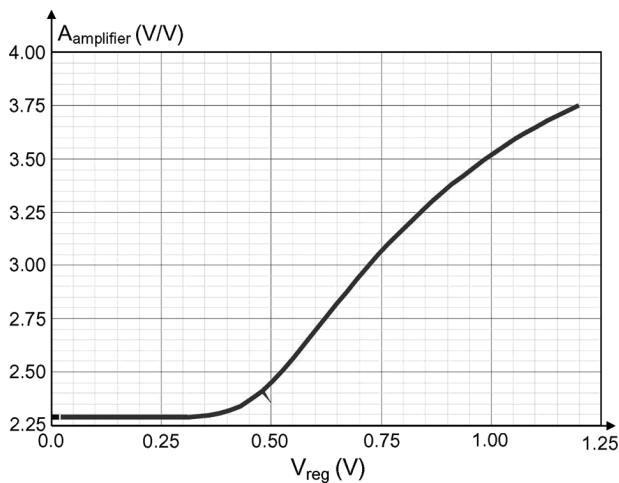
Fig. 10.   Schematic of the amplitude regulator.



Fig. 11.   Gain of the amplifier as function of the voltage applied to the bridge transistor.



Fig. 12.   Complete schematic of the Wienbridge oscillator. The gain boost amplifiers are omitted for clarity reasons.

(Fig. 10). If the peaks are too high, the signal will leak through the source of the peak-detecting transistors $T_{c,1}$, $T_{c,2}$. When the regulator network is in stable operation, only a very small peak current is running through these transistors which makes the input impedance of the measuring circuit very high. The increased leakage current over temperature causes a small linear temperature coefficient of the input impedance. The larger the peak detection transistors, the more stable the amplitude regulator but the higher the temperature dependent leakage current will be. Good results where obtained with a transistor size of $3 \times 0.65\,\mu\text{m}/3\,\mu\text{m}$. In Section VII, a solution to this small temperature dependency will be described.

The adaptation of the gain can be done by a transistor between the two differential amplifier branches. This transistor controls the resulting source degeneration resistance, which in turn controls the gain. One very beneficial property of this technique is that it does not influence the DC-operating point of the circuit, only the AC-gain is altered in this way. The influence on the output resistance is negligible due to the shielding by the gain-boosted cascode transistors. Fig. 11 shows the voltage gain as a function of the gate voltage of the 'bridge' transistor. By using a transistor of $W/L = 0.3\,\mu\text{m}/0.1\,\mu\text{m}$, a very wide tuning range ($A = 2.25\dots 3.5$) is obtained.
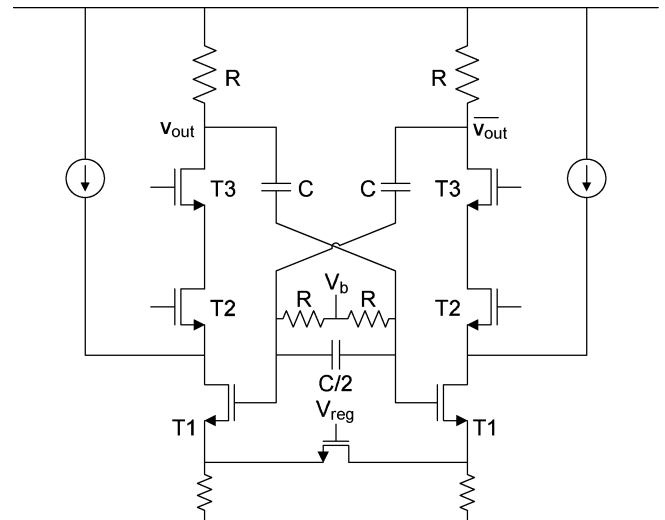
The complete regulation circuit with peak detection transistors $T_{c,1}$ and $T_{c,2}$, integration capacitor $C$, amplifier replica and feedback amplifier is shown in Fig. 10.

### C. Complete Circuit

Using the different components discussed in the previous sections, the complete oscillator can be constructed. The full schematic can be seen in Fig. 12, in which the gainboosting amplifiers and the amplitude regulator circuit have been left out, to increase clarity. The current drawn by the input transistor is 10 $\mu$A, of which 60% is flowing through the cascode transistors. The remaining 40% is supplied through the current bleeding. The total power consumption, biasing included, is 66 $\mu$W at a supply voltage of 1.2 V. The feedback circuit, with a resistor value of 50 k$\Omega$ and capacitor value of 530 fF, is designed to obtain an oscillation frequency of 6 MHz.

At both outputs, two cascaded source followers have been added to provide sufficient buffering of the signal.

### VI. PHASE NOISE PERFORMANCE

Although the circuit was not designed for phase noise performance, it is interesting to identify the different noise sources. In this way it is possible to predict the noise behavior as a function of the power consumption and other design parameters. Also the difference between the standard, single loop topology and the differential structure presented in this paper, is calculated.

### A. Noise in the Transconductance Amplifier

In a first step the resulting noise of the transconductance amplifier is modeled as a single current noise source at the output. This equivalent noise current is a combination of the most important noise sources in the amplifier (Fig. 13). Three different noise sources are drawn, the first is a voltage source $v_{n,1/f}$ at the input, which represents the flicker noise at the gate-semiconductor interface. Furthermore two current sources are indicated,
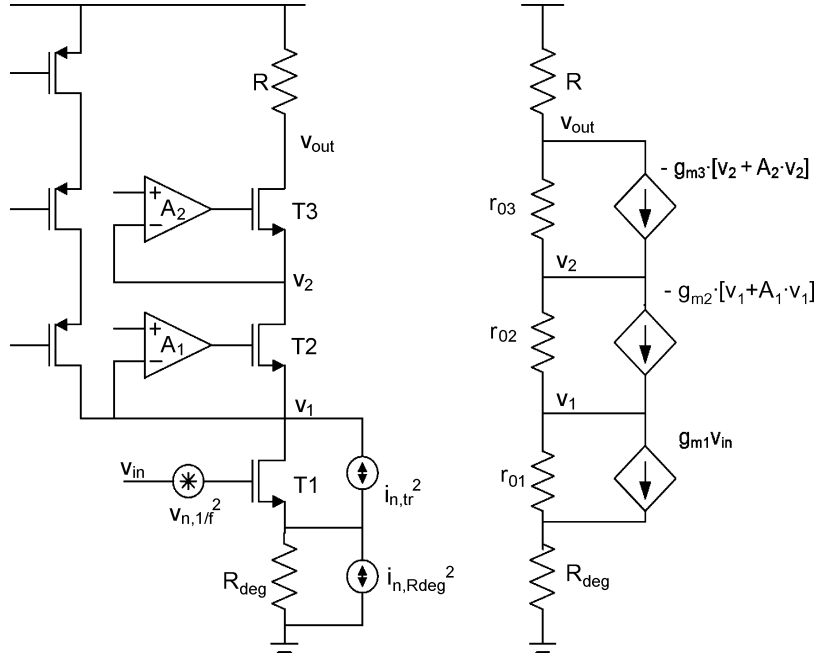
Fig. 13. Main noise sources in the transconductance amplifier.

$i_{n,tr}$ and $i_{n,R_{\deg}}$, which represent the channel noise and the resistor noise respectively. As stated in [10], the noise of the cascode transistors and gain-boosters is negligible compared to the noise of the input transistor. Because of the fact that the current sources for the current bleeding are not conducting any AC-current, their dimensions and output resistance can be maximized in order to minimize the noise. This makes them negligible in the noise calculation. Apart from the input transistor, the degeneration resistor at the source of the input transistor also contributes to the noise in the output current.

Consequently, the transfer functions of the different noise sources to the amplifiers output current can be calculated. The resulting noise contribution of the source resistor to the output noise is given by

$$i_{n,R_{\deg}}^2 = \frac{4kT}{R_{\deg}} \cdot \left(\frac{g_m R_{\deg}}{1 + g_m R_{\deg}}\right)^2 = \frac{4kT g_m^2 R_{\deg}}{(1 + g_m R_{\deg})^2} \quad (17)$$

where $k$ is the Boltzman constant. The noise contribution from the transistor itself is caused by two complementary sources. The flicker noise is

$$i_{n,tr,1/f}^2 = \frac{K}{WLC_{ox}f} \cdot \frac{g_m^2}{(1 + g_m R_{\deg})^2} \quad (18)$$

which is inversely proportional to f and where K is a transistor parameter dependent on the technology node. The other contribution of the input transistor is white channel noise and is given by

$$i_{n,tr}^2 = \frac{8kT}{3g_m} \cdot \left(\frac{g_m}{1 + g_m R_{\deg}}\right)^2 = \frac{8kT g_m}{3 \cdot (1 + g_m R_{\deg})^2}. \quad (19)$$

Note that the input transistors are rather large ($W/L = 5 \times 0.5$ $\mu$m/3.4 $\mu$m) to enhance their flicker noise behavior and eliminate the short channel effects, which also have an influence on the transistor noise. The rms current of the resulting noise
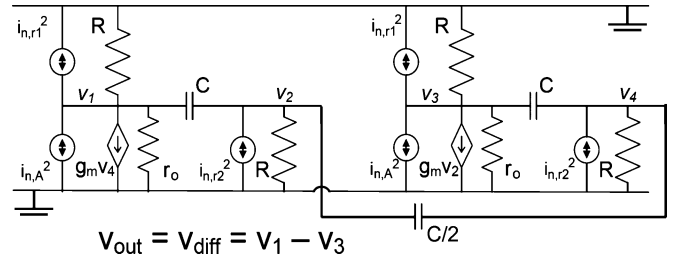


Fig. 14. Small signal schematic of the differential oscillator. The noise contributions of the amplifier are grouped in $i_{n,A}^2$.

source at the output of the transconductance amplifier can be calculated as the sum of these 3 contributions.

### B. Noise Propagation in the Feedback Network

The noise of these different noise sources (amplifier and resistors in the feedback network) is then propagated and filtered by the feedback network. To calculate the different noise contributions to the output, it is necessary to calculate the transfer function of the feedback system from their injection points to the differential output. The small signal network including the different noise-current sources is given in Fig. 14. In this figure $i_{n,A}^2$ represents the estimated resulting noise contribution of the amplifier. Starting from this circuit and supposing that the voltage gain of each amplifier is equal to 3, the transfer functions from the noise sources to the output can be derived. The transfer function for the noise source ($i_{n,r_2}^2$) to the differential output is given by

$$H_{n1}(s) = \frac{-(sRC + 3)R}{s^2 R^2 C^2 + 1}. \quad (20)$$

The transfer function for a current source at the output of the transconductance amplifier (the noise contribution of the output
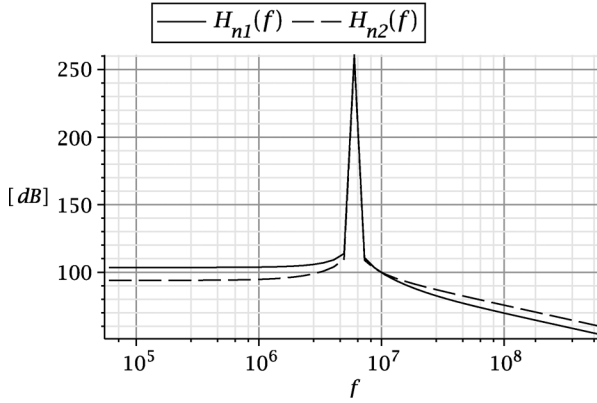
Fig. 15. Bodeplot of the noise transfer functions. The sharp peak is the resonant frequency of the closed loop system.
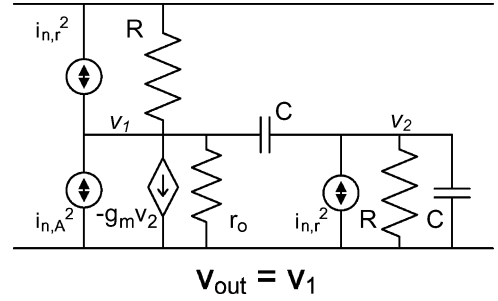


Fig. 16. Small signal schematic of a single-ended wienbridge oscillator. The propagation of the amplifier noise to the output is proved to be the same as in the differential case.

resistance $(i_{n,r_1}^2)$ and the amplifier itself $(i_{n,A}^2)$) to the differential output is equal to

$$H_{n2}(s) = \frac{-(2sRC+1)\cdot R}{s^2 R^2 C^2 + 1}. \tag{21}$$

Note that in case of a constant oscillation frequency, the transfer function is proportional to the resistor $R$ in the feedback network. The noise transfer functions are plotted in Fig. 15. These transfer functions are also valid for the noise sources in a single ended system (Fig. 16). The differential system contains twice as much noise sources than the single ended oscillator. Due to the double output amplitude, the SNR at the output is exactly the same in both circuits. Important benefits of the differential structure compared to the single ended structure are a lower sensitivity to supply and ground noise and a lower distortion of the output signal.

### C. Resulting Output Noise

The noise value at the differential outputs can be calculated as the overall noise power of the different noise sources. Each noise contribution is multiplied by 2 and by its transfer function. The noise at the differential output is then approximated by

$$V_{n,diff}^2 = \left( \frac{K}{WLC_{ox}f} \cdot \frac{g_m^2}{(1+g_m R)^2} + \frac{4kT g_m^2 R_{\deg}}{(1+g_m R_{\deg})^2} \right.$$
$$\left. + \frac{8kT g_m}{3\cdot(1+g_m R)^2} + \frac{4kT}{R} \right) \cdot 2 \cdot |H_{n2}(s)|^2$$
$$+ \frac{4kT}{R} \cdot 2 \cdot |H_{n1}(s)|^2 \tag{22}$$

The first term in this equation is inversely proportional to the third power of the frequency. This contribution to the noise at the output, and consequently also to the phase noise, is most important at frequencies near to the oscillation frequency. The other contributions are inversely proportional to the square of the frequency. Their contributions become more important at frequencies further away from the oscillation frequency.

An important question is what will happen to a design with a different current in the amplifier. When the frequency is kept constant and the DC voltages of the circuit remain equal, $g_m$ is proportional to the current and inversely proportional to the resistors $R$ and $R_{\deg}$ in the amplifiers. As a result the gain of the amplifiers will not change and the Barkhausen criterion remains

fulfilled. Since the frequency is a constant and proportional to $R \cdot C$, $R$ is inversely proportional to $C$.

$$g_m \sim C \sim I_{ds} \tag{23}$$
$$R \sim R_{\deg} \sim 1/I_{ds} \tag{24}$$

When the biasing current is doubled, the noise transfer functions are divided by two. Supposing the active area $(W \cdot L)$ of the input transistor scales linearly with the current (the transistor length stays constant), the contribution of the transistor flicker noise is inversely proportional to the power consumption. Moreover, the contributions of the resistors and transistor to the total noise power are inversely proportional to the drain-source current of the input transistor. To enhance the phase noise at frequencies close to the output frequency, the width of the input transistor has to be enlarged. Considering Fig. 9, this can be done as long as the amplifier bandwidth is high enough and its phase shift remains negligible. For a fixed power consumption, one can also lower the noise by changing the DC biasing of the circuit. By lowering the resistors for a given current, however, the output amplitude is decreased. This keeps the SNR value at the output almost constant.

In Section VII-B, the measured phase noise performance is discussed.

## VII. MEASUREMENT RESULTS

The complete circuit has been designed and processed in a 65 nm mixed signal/RF CMOS technology. The capacitors used are MIM-capacitors. Resistors are implemented as a combination of N- and P-poly resistors. Note that no trimming or calibration has been used. The active area of the chip, including biasing and output buffers, measures 200 $\mu$m $\times$ 150 $\mu$m and is shown in Fig. 17.

### A. Temperature Stability

During measurements, 7 samples from one batch have been characterized. The oscillation frequency is 5.998 MHz with a standard deviation of 53 kHz (0.88%), both measured at room temperature. Fig. 18 shows the temperature dependency of the oscillation frequency for different samples in a temperature range from 0 to 100°C. A linear frequency dependency of 86.1 ppm/°C exists, which corresponds very well to the simulated value of 81–92 ppm/°C, including process corners. This temperature dependency is mostly due to the input resistance of the amplitude regulator. However, this dependency can be
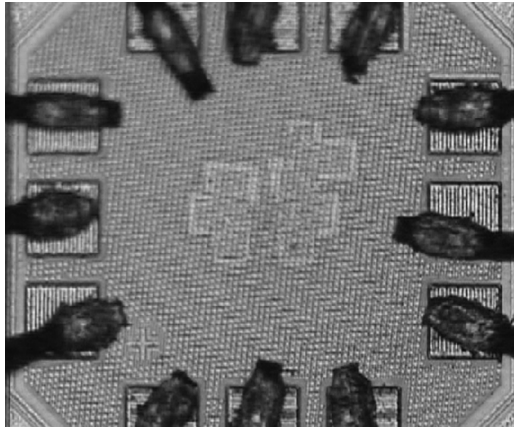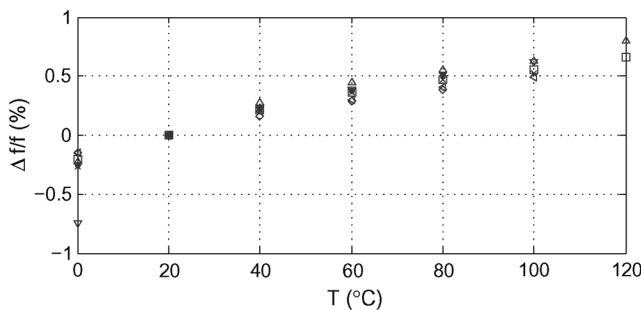
Fig. 17. Chip photograph.



Fig. 19. Measured phase noise as a function of carrier offset for 3 different samples.



Fig. 18. Measured frequency deviation as a function of temperature for different samples. The frequency was normalized at 20°C, some samples did not work at 120°C.

TABLE I
OVERVIEW OF SOME KEY PROPERTIES

| Technology | 65$nm$ CMOS |
|---|---|
| Frequency | 5.998 MHz |
| Power consumption | 66 $\mu$W |
| Temperature Coefficient | 86, 1 ppm/$^\circ$C |
| Absolute Accuracy | 53 kHz (0.88%) |
| Phase Noise | −73, 7 dBc/Hz@10kHz |
| | −94.6 dBc/Hz@100kHz |
| Phase Noise FOM | 172 dB |
| Area | 200 $\mu$m × 150 $\mu$m |

compensated by the resistors (Section VII-C). The amplitude of the output signal remains constant, proving correct operation of the amplitude regulator.

### B. Noise Performance

In addition to the frequency stability, the phase noise of the oscillator (as defined by [3], eq. (2)) is also extracted with a single-sideband measurement using a Rhode and Schwarz FSIQ26 Spectrum Analyzer. In Fig. 19, the measured phase noise density $(L(f_m))$ is represented as a function of the frequency offset from the carrier $(f_m)$ for three of the measured samples. The noise measurements are made at room temperature. At an offset frequency of 10 kHz and 100 kHz a phase noise of respectively −73,7 dBc/Hz and −94,6 dBc/Hz is measured at the output of the chip. On this figure, the simulated noise is also indicated (thick black line). Apparently, the measurements correspond very well to the simulations.

To compare the phase noise performance with other designs, the Figure of Merit presented in [6] is calculated. This FOM compares the noise performance at a relative frequency offset to the power consumption $P_{\text{diss}}$ of the circuit. Considering the conclusions of Section VI-C, increasing the oscillator power consumption will not have any influence on the FOM. At a frequency offset of 100 kHz, the following result is obtained:

$$\text{FOM} = 10 \cdot \log\left(\frac{f_{\text{osc}}^2}{f_m^2 \cdot L(f_m)} \cdot \frac{1}{P_{\text{diss}}}\right) = 172 \text{ dB} \quad (25)$$
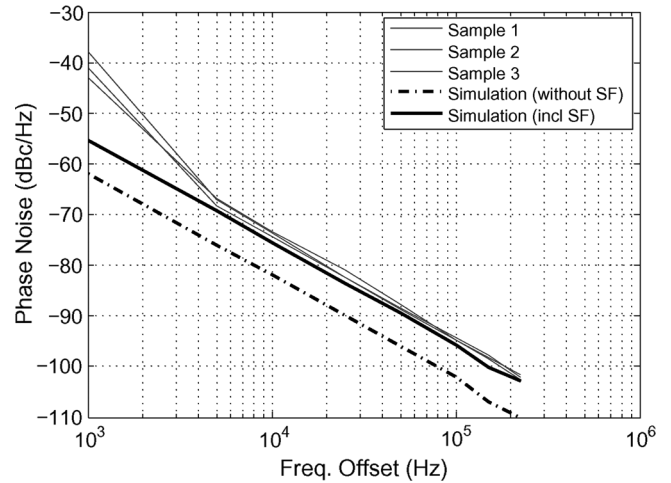
Note that the measured data includes the noise added by source followers (SF), used as output buffers, on the chip. Since the noise performance of a source follower is very poor [10], the intrinsic noise performance of the oscillator is much better. The simulated noise of the oscillator itself, without the source followers as output buffer, is 8 dB below the phase noise at the output of the source followers. In this case, the equivalent value of the oscillators phase noise FOM at a frequency offset of 100 kHz is

$$\text{FOM} = 10 \cdot log\left(\frac{f_{\text{osc}}^2}{f_m^2 \cdot L(f_m)} \cdot \frac{1}{P_{\text{diss}}}\right) = 180 \text{ dB}. \quad (26)$$

### C. Suggested Improvements

Since the simulated temperature behavior corresponds very well to the measured behavior, an improvement to the temperature dependency of the measured circuit is simulated. In this circuit, the temperature coefficient of the amplitude regulator is compensated by adding an opposite, first-order temperature coefficient in the resistors of the feedback network. This results in a simulated temperature dependence of 28–33 ppm/$^\circ$C, which corresponds to the second-order temperature coefficient of the resistors (36 ppm/$^\circ$C). Remind that the reported frequency mismatch is far below the predicted values in Section III-B. However, some more samples should be measured to characterize the wafer-to-wafer mismatch accurately.

TABLE II
COMPARISON TO THE STATE-OF-THE-ART

| Ref. | Type | Tech. | f (MHz) | T Sens. (ppm/°C) | P | FOM (dB, eq. 25) | Trimming/Calibration? |
|------|------|-------|---------|------------------|---|------------------|-----------------------|
| This Work | RC | 65 nm | 6 | 86 | 66 μW | 172 (180) | No |
| [19] | LC | 0.35 μm | 12 | 12 | 31 mW | 180 | No |
| [20] | relaxation | 0.5 μm | 4 − 22 | 460 | 400 μW | | Yes |
| [21] | ring | 0.6 μm | 0.68 | 106 | 400 μW | | No |
| [22] | ring | 0.25 μm | 7 | 400 | 1.5 mW | | No |
| [5] | relaxation | 65 nm | 12 | | 90 μW | 162 | No |
| [6] | relaxation | 0.8 μm | 1.5 | | 1.8 mW | 150,7 | No |
| [23] | relaxation | 1.2 μm | 148 | 1000 | 1.1 mW | 176 | No |
| [7] | relaxation | 65 nm | 0.1 | 103 | 41.2 μW | | Ext. Ref. |
| [24] | relaxation | 0.13 μm | 2 | 375 | 3 μW | 169.7 | Yes |

### D. Comparison to the State of the Art

An overview of the most important properties of the circuit is listed in Table I. In Table II, a comparison is made between the presented circuit and some recently published temperature stable and low noise oscillators. The proposed topology appears to perform very well in a deep-sub-micron CMOS technology. The temperature stability at an ultra-low power consumption is high compared to the other references. Compared to other low-Q resonators and relaxation oscillators, the phase noise performance is rather good [4], [5], [12]. Note that no trimming or calibration was used to get the reported results.

## VIII. CONCLUSION

An improved Wienbridge topology has been developed, realizing a fully-integrated, low-power (66 μW), precise ($\sigma_{f_{osc}} = 0.88\%$), temperature-independent (86.1 ppm/°C) oscillator. Advanced design techniques have been used to obtain a high performance oscillator, of which the specifications are listed in Table I. The measured temperature dependency and phase noise performance correspond very well to the simulated values.

### ACKNOWLEDGMENT

### REFERENCES

[1] P. Bruschi, N. Nizza, and M. Dei, "A low-power capacitance to pulse width converter for MEMS interfacing," in *Proc. European Solid-State Circuits Conf. (ESSCIRC)*, Sept. 2008, pp. 446–449.

[2] J. Rabaey, J. Ammer, T. Karalar, S. Li, B. Otis, M. Sheets, and T. Tuan, "Picoradios for wireless sensor networks: The next challenge in ultra-low-power design," in *IEEE Int. Solid-State Circuits Conf. (ISSCC) Dig. Tech. Papers*, 2002, vol. 2, pp. 156–445.

[3] A. Hajimiri and T. Lee, "A general theory of phase noise in electrical oscillators," *IEEE J. Solid-State Circuits*, vol. 33, no. 2, pp. 179–194, Feb. 1998.

[4] T. Lee and A. Hajimiri, "Oscillator phase noise: A tutorial," *IEEE J. Solid-State Circuits*, vol. 35, no. 3, pp. 326–336, Mar. 2000.

[5] P. Geraedts, E. van Tuijl, E. Klumperink, G. Wienk, and B. Nauta, "A 90 μW 12 MHz relaxation oscillator with a −162 dB FOM," in *IEEE Int. Solid-State Circuits Conf. (ISSCC) Dig. Tech. Papers*, 2008, pp. 348–618.

[6] S. Gierkink and E. van Tuij, "A coupled sawtooth oscillator combining low jitter with high control linearity," *IEEE J. Solid-State Circuits*, vol. 37, no. 6, pp. 702–710, Jun. 2002.

[7] F. Sebastiano, L. Breems, K. Makinwa, S. Drago, D. Leenaerts, and B. Nauta, "A low-voltage mobility-based frequency reference for crystal-less ULP radios," in *Proc. European Solid-State Circuits Conf. (ESSCIRC)*, 2008, pp. 306–309.

[8] J. Ryckaert, M. Verhelst, M. Badaroglu, S. D'Amico, V. De Heyn, C. Desset, P. Nuzzo, B. Van Poucke, P. Wambacq, A. Baschirotto, W. Dehaene, and G. Van der Plas, "A CMOS ultra-wideband receiver for low data-rate communication," *IEEE J. Solid-State Circuits*, vol. 42, no. 11, pp. 2515–2527, Nov. 2007.

[9] K. Clarke, "Wien bridge oscillator design," *Proc. IRE*, vol. 41, no. 2, pp. 246–249, Feb. 1953.

[10] W. Sansen, *Analog Design Essentials*. New York: Springer, 2006.

[11] A. Budak and K. Nay, "Operational amplifier circuits for the Wien-bridge oscillator," *IEEE Trans. Circuits Syst.*, vol. 28, no. 9, pp. 930–934, Sep. 1981.

[12] B. Razavi, "A study of phase noise in CMOS oscillators," *IEEE J. Solid-State Circuits*, vol. 31, no. 3, pp. 331–343, Mar. 1996.

[13] P. B. Y. Tan, A. V. Kordesch, and O. Sidek, "Analysis of poly resistor mismatch," in *IEEE Int. Conf. Semiconductor Electronics, 2006 (ICSE '06)*, 2006, pp. 1028–1029.

[14] Y. Cheng, "The influence and modeling of process variation and device mismatch for analog/rf circuit design," in *Proc. 4th IEEE Int. Caracas Conf. Devices, Circuits and Systems*, 2002, pp. D046-1–D046-8.

[15] J. Lin, T. Yeh, C. Lee, C. Chen, J. Tsay, S. Chen, H. Hsu, C. Chen, C. Huang, J. Chiang, A. Chang, R. Chang, C. Chang, S. Wang, C. Wu, C. Lin, Y. Chu, S. Chen, C. Hsu, R. Liou, S. Wong, D. Tang, and J. Sun, "State-of-the-art rf/analog foundry technology," in *Proc. Bipolar/BiCMOS Circuits and Technology Meeting*, 2002, pp. 73–79.

[16] M. Pelgrom, A. Duinmaijer, and A. Welbers, "Matching properties of MOS transistors," *IEEE J. Solid-State Circuits*, vol. 24, no. 5, pp. 1433–1439, Oct. 1989.

[17] E. Vannerson and K. Smith, "Fast amplitude stabilization of an RC oscillator," *IEEE J. Solid-State Circuits*, vol. 9, no. 4, pp. 176–179, Aug. 1974.

[18] V. De Smedt, P. De Wit, W. Vereecken, and M. Steyaert, "A fully-integrated Wienbridge topology for ultra-low-power 86 ppm/°C 65 nm CMOS 6 MHz clock reference with amplitude regulation," in *Proc. European Solid-State Circuits Conf. (ESSCIRC)*, 2008.

[19] M. McCorquodale, "Self-referenced, trimmed and compensated RF CMOS harmonic oscillators as monolithic frequency generators," in *IEEE Int. Frequency Control Symp.*, 2008, pp. 408–413.

[20] A. Boas, J. Soldera, and A. Olmos, "A 1.8 V supply multi-frequency digitally trimmable on-chip IC oscillator with low-voltage detection capability," in *Proc. 17th Symp. Integrated Circuits and Systems Design (SBCCI 2004)*, 2004, pp. 44–48.

[21] Y.-S. Shyu and J.-C. Wu, "A process and temperature compensated ring oscillator," in *Proc. 1st IEEE Asia Pacific Conf. ASICs (AP-ASIC '99)*, 1999, pp. 283–286.

[22] K. Sundaresan, P. Allen, and F. Ayazi, "Process and temperature compensation in a 7-MHz CMOS clock oscillator," *IEEE J. Solid-State Circuits*, vol. 41, no. 2, pp. 433–442, Feb. 2006.

[23] Y. Deval, J. Tomas, J. Begueret, H. Lapuyade, and J. Dom, "1-V low-noise 200 MHz relaxation oscillator," in *Proc. European Solid-State Circuits Conf. (ESSCIRC)*, 1997, pp. 220–223.

[24] M. Paavola, M. Laiho, M. Saukoski, and K. Halonen, "A 3/spl mu/W, 2 MHz CMOS frequency reference for capacitive sensor applications," in *Proc. IEEE Int. Symp. Circuits and Systems (ISCAS)*, 2006, p. 4.

**Wim Vereecken** (M'08) received the M.S. and Ph.D. degrees in electrical engineering from the Katholieke Universiteit Leuven (K.U.Leuven), Belgium, in 2002 and 2008, respectively. His Ph.D. thesis was titled "Pulse-Based Radio: Reliable Communication over a Wideband Channel" and was in collaboration with the Mixed Signal Circuits & Systems Group of NXP Semiconductors in Eindhoven, The Netherlands.

He currently holds an industrial postdoctoral position with the K.U.Leuven, where his research is in the area of analog CMOS RF design.



**Valentijn De Smedt** (S'08) was born in Lubbeek, Belgium, in 1984. He received the M.Sc. degree in electrical engineering from the Katholieke Universiteit Leuven, Belgium, in 2007. The subject of his M.S. thesis was on the design of an accurate integrated frequency reference. He is currently working as a research assistant at the MICAS laboratories of the Katholieke Universiteit Leuven, pursuing the PhD degree on the design of ultra-low-power UWB transmitters for wireless sensor networks.



**Michel S. J. Steyaert** (F'03) received the Masters degree in electrical–mechanical engineering and the Ph.D. degree in electronics from the Katholieke Universiteit Leuven (K.U.Leuven), Heverlee, Belgium, in 1983 and 1987, respectively.

From 1983 to 1986 he obtained an IWNOL fellowship (Belgian National Foundation for Industrial Research) which allowed him to work as a Research Assistant at the Laboratory ESAT at K.U.Leuven. In 1987 he was responsible for several industrial projects in the field of analog micro power circuits at the Laboratory ESAT as an IWONL Project Researcher. In 1988 he was a Visiting Assistant Professor at the University of California, Los Angeles. In 1989 he was appointed by the National Fund of Scientific Research (Belgium) as Research Associate, in 1992 as a Senior Research Associate and in 1996 as a Research Director at the Laboratory ESAT, K.U.Leuven. Between 1989 and 1996 he was also a part-time Associate Professor. He is now a Full Professor at the K.U.Leuven and the Chair of the Electrical Engineering Department. His current research interests are in high-performance and high-frequency analog integrated circuits for telecommunication systems and analog signal processing.

Prof. Steyaert authored or co-authored over 400 papers in international journals or proceedings and co-authored over 15 books. He received the 1990 and 2001 European Solid-State Circuits Conference Best Paper Award. He received the 1991 and the 2000 NFWO Alcatel-Bell-Telephone award for innovative work in integrated circuits for telecommunications. He received the 1995 and 1997 IEEE-ISSCC Evening Session Award and the 1999 IEEE Circuit and Systems Society Guillemin-Cauer Award. He was also recognized as one of the top 10 authors in the 50-year history of ISSCC.



**Pieter De Wit** (S'06) was born in Wilrijk, Belgium, in 1984. He received the M.Sc. degree in electrical engineering from the Katholieke Universiteit Leuven in 2007. He is currently a Research Assistant working towards the Ph.D. degree at the ESAT-MICAS Laboratory of the same university.

His research focuses on the design of reconfigurable, mixed-signal integrated circuits.